



# Boron-doped single crystal $\text{LiNi}_{0.6}\text{Mn}_{0.2}\text{Co}_{0.2}\text{O}_2$ with improved electrochemical performance for lithium-ion batteries

Bing Huang<sup>1</sup> · Xiaowei Yang<sup>1</sup> · Guodong Xu<sup>1</sup> · Meng Wang<sup>2</sup> · Yijie Gu<sup>3</sup>

Received: 12 June 2019 / Revised: 30 June 2019 / Accepted: 8 July 2019 / Published online: 24 July 2019  
© Springer-Verlag GmbH Germany, part of Springer Nature 2019

## Abstract

Single crystal boron-doped  $\text{LiNi}_{0.6}\text{Mn}_{0.2}\text{Co}_{0.2}\text{O}_2$  cathode material with excellent electrochemical properties were synthesized in the study. X-ray diffraction revealed that boron doping promoted the unit cell expands along the *c*-direction which was conducive to improving the kinetic of lithium-ion transmission. Electrochemical tests showed that boron-doped cathode material exhibited remarkable improvement in cycling performance and rate capability compared to bare sample. After 50 cycles at 1.0 C, the boron-doped sample delivered  $176.3 \text{ mAh g}^{-1}$  with a retention of 96.1%, which was much higher than that of the undoped sample of  $167.8 \text{ mAh g}^{-1}$  with a retention of 90.7%. The highly ordered layered structure and improved structure stability during repeated intercalation/deintercalation of lithium ions were responsible for the enhanced electrochemical performance. Besides that, the unique single crystal morphology resulted in even faster lithium-ion transportation as a result of small particle size. Both the doping effects of boron and single crystal particles contributed to the excellent electrochemical performance of the doped cathode materials.

**Keywords** Single crystal morphology · Boron doping · Lithium-ions diffusion · Lithium-ion batteries

## Introduction

Increasing demand for high-energy-density lithium-ion batteries has prompted researchers to explore high-performance cathode materials. Although various new classes of materials have been developed in the last decades,  $\text{LiNi}_x\text{Co}_y\text{Mn}_{1-x-y}\text{O}_2$  ( $x \geq 0.6$ ) layered oxides still dominating the main commercial market due to their relatively low cost, high capacity, and excellent rate capability. In recent years, the focus of research in  $\text{LiNi}_x\text{Co}_y\text{Mn}_{1-x-y}\text{O}_2$ -layered oxides have shifted to the high volume energy density and application at high voltages, which can increase its capacity and energy density. However, these

materials still undergo severe property degradation in the process of charge/discharge, such as voltage reduction and structural transformation, especially at high voltages ( $> 4.3 \text{ V}$ ) [1–4]. In recent years, considerable effects have been devoted to stabilizing crystal structure and improving electrochemical performance of the cathode materials, such as surface coating, bulk phase doping, and reducing the particle size.

Coating the surface of cathode materials with  $\text{Al}_2\text{O}_3$ ,  $\text{TiO}_2$ ,  $\text{MnO}_2$ ,  $\text{Li}_3\text{PO}_4$ , and  $\text{Li}_3\text{VO}_4$ -PPy can effectively improve the host structure of cathode materials against HF attack and reduce the side reactions between electrode and electrolyte [5–9]. Meanwhile, bulk phase doping with  $\text{Al}^{3+}$ ,  $\text{Zr}^{4+}$ , and  $\text{Mg}^{2+}$  are effective strategies to stabilize the crystal structure and minimize the capacity and voltage decay [10–12]. There are some reports about boron is doped in  $\text{LiCoO}_2$ ,  $\text{LiV}_3\text{O}_8$ ,  $\text{LiMn}_2\text{O}_4$ ,  $\text{LiMnPO}_4$ ,  $\text{Li}(\text{Li}_{0.2}\text{Ni}_{0.13}\text{Co}_{0.13}\text{Mn}_{0.54})\text{O}_2$ , and the results show that boron doping stabilizes the structure of cathode materials and improves electrochemical performance [13–16]. Alcantara et al. [17] first reported an improved reversibility of lithium (de)intercalation in  $\text{LiCo}_{0.95}\text{B}_{0.05}\text{O}_2$  and proposed a tetrahedral coordination for boron. Feng et al. [14] proved boron doping can enlarge crystal layers of  $\text{LiV}_3\text{O}_8$  and improve the structural stability during intercalation/deintercalation of lithium ions in material. Ebin et al. [15]

✉ Meng Wang  
manyou2005@163.com

✉ Yijie Gu  
guyijie@sdust.edu.cn

<sup>1</sup> Institute of New Energy on Chemical Storage and Power Sources, Yancheng Teachers University, Yancheng 224000, China

<sup>2</sup> China Academy of Machinery Science and Technology Group Co. Ltd., Beijing 100044, China

<sup>3</sup> School of mechanical-electronic and vehicle Engineering, Weifang University, Weifang 261061, China

reported boron was an electron-deficient element and its substitution into  $\text{LiMn}_2\text{O}_4$  can strain the spinel lattice due to its small ionic radius ( $\text{B}^{3+} = 40$  pm) compared to  $\text{Mn}^{3+}$  and  $\text{Mn}^{4+}$  ( $\text{Mn}^{3+} = 72$  pm,  $\text{Mn}^{4+} = 67$  pm) and therefore leads to better cycling performance. There are some studies about incorporating small amount of boron doping in Li-rich cathode materials block the migration channel of transition metal ions and stabilize the crystal structure [18–20]. Besides that, it showed boron doping facilitates the formation of layered structures by lowering the crystallization temperature of the layered structure [21]. Based on the above analysis, the cycle stability of  $\text{LiNi}_x\text{Co}_y\text{Mn}_{1-x-y}\text{O}_2$  is expected to be enhanced by boron doping. However, there are few studies that focus on the boron doping in  $\text{LiNi}_x\text{Co}_y\text{Mn}_{1-x-y}\text{O}_2$ . This study attempts to improve the cycling performance of  $\text{LiNi}_x\text{Co}_y\text{Mn}_{1-x-y}\text{O}_2$  through boron doping.

Morphology, particle size, and the corresponding specific surface area are also critical to the electrochemical performance of the materials [22–24]. Small particle size can significantly shorten the diffusion distance length and increase electrode/electrolyte contact area, and thus resulting in a fast lithium-ion transfer in cathode materials [25–27]. However, almost all the reported  $\text{LiNi}_x\text{Co}_y\text{Mn}_{1-x-y}\text{O}_2$  are micron-sized secondary aggregated particles, rather than single crystal particles like  $\text{LiCoO}_2$ . Such large aggregate particles will lead to a long path of lithium-ion diffusion and adversely affects the tap density, which is not conducive to the rate performance and volume energy of the cathode materials [28]. Small particles are helpful for the rate capability improvement because of the short path for lithium diffusion inside the particles. But too small particles are detrimental to the cyclic stability due to the increased contact area between cathode materials and electrolyte, which might accelerate the decomposition of electrolyte and the dissolution of cathode materials. Consequently, preparing single crystal particles with several micron size can effectively promote the rapid migration of lithium ions in the material and thus improve electrochemical properties of cathode materials. However, it is difficult to synthesize single-crystal  $\text{LiNi}_x\text{Co}_y\text{Mn}_{1-x-y}\text{O}_2$  particles with excellent electrochemical properties for they are composed of three transition metal ions. Therefore, there are few reports on successful preparation of  $\text{LiNi}_x\text{Co}_y\text{Mn}_{1-x-y}\text{O}_2$  with single crystal particles.

Based on the above analysis, the advantages of boron doping and single crystal morphology are combined to prepare the excellent boron-doped  $\text{LiNi}_{0.6}\text{Mn}_{0.2}\text{Co}_{0.2}\text{O}_2$  in this study. Boron doping promises good cycling performance and easy fabrication, while single crystal morphology provides short diffusion lengths for lithium ions and high tap density. In summary, layered boron-doped  $\text{LiNi}_{0.6}\text{Mn}_{0.2}\text{Co}_{0.2}\text{O}_2$  with single crystal morphology can be synthesized through our method. The work provides a new way to further improve the electrochemical performance of  $\text{LiNi}_x\text{Co}_y\text{Mn}_{1-x-y}\text{O}_2$ .

## Experimental

### Material synthesis

The  $\text{Ni}_{0.6}\text{Mn}_{0.2}\text{Co}_{0.2}(\text{OH})_2$  precursor was conventional commercial materials. Five grams of  $\text{Ni}_{0.6}\text{Mn}_{0.2}\text{Co}_{0.2}(\text{OH})_2$  was precalcined at 700 °C for 5 h to form  $\text{Ni}_{0.6}\text{Mn}_{0.2}\text{Co}_{0.2}\text{O}_2$ , then it was mixed with 5% excess  $\text{Li}_2\text{CO}_3$  and 0.025 g and 0.05 g  $\text{B}_2\text{O}_3$ , respectively. The mixture was annealed at 920 °C for 5 h and 940 °C for 2 h to obtain agglomerated B-doped materials (named as A-0.5 and A-1.0). The obtained sample A-0.5 and A-1.0 was then ball milled at 500  $\text{r min}^{-1}$  for 1 h and reheated at 800 °C for 3 h to get the single-crystal B-doped materials (named as S-0.5 and S-1.0). For comparison, we prepared  $\text{LiNi}_{0.6}\text{Mn}_{0.2}\text{Co}_{0.2}\text{O}_2$  by the same preparation method, and the agglomerated sample before ball milling was named as A-0.0, while the obtained single-crystal sample after being reheated was named as S-0.0.

### Material characterizations

X-ray diffraction (XRD) patterns of the samples were performed on a Rigaku Ultima IV-185 (Cu  $\text{K}\alpha$  radiation) between 10 and 80° 2 $\theta$  at a scan rate of 8°  $\text{min}^{-1}$ . The morphology of materials was observed by a FEI Quanta 250 field emission scanning electron microscope (FESEM) on a HORIBA EMAX instrument. And the distribution of elements on the surface of a single particle was observed by energy-dispersive spectroscopy (EDS) on a HITACHI SU8020.

### Electrochemical measurements

The electrochemical performances of the materials were tested using a CR2025 type coin cell. The cathode electrodes were prepared by casting a mixture containing 85 wt.% active materials, 10 wt.% acetylene black, and 5 wt.% polyvinylidene fluoride on Al current collector foil. The counter electrode is lithium metal foil, the separator is Celgard 2400 film, and 1 M  $\text{LiPF}_6$  in ethylene carbonate (EC)-dimethyl carbonate (DMC) (1:1, v/v) as the electrolyte. Electrochemical measurements were performed between 2.8 and 4.5 V on Land CT2001A. Electrochemical impedance spectroscopy (EIS) measurements were carried out using a CHI604D impedance analyzer, with an amplitude voltage of 5 mV and the frequency range of  $10^{-2}$ – $10^5$  Hz.

## Results and discussion

### Morphology and structural analysis

Figure 1 shows FESEM of agglomerated samples (A-0.0, A-0.5, and A-1.0) and single-crystal samples (S-0.0, S-0.5,

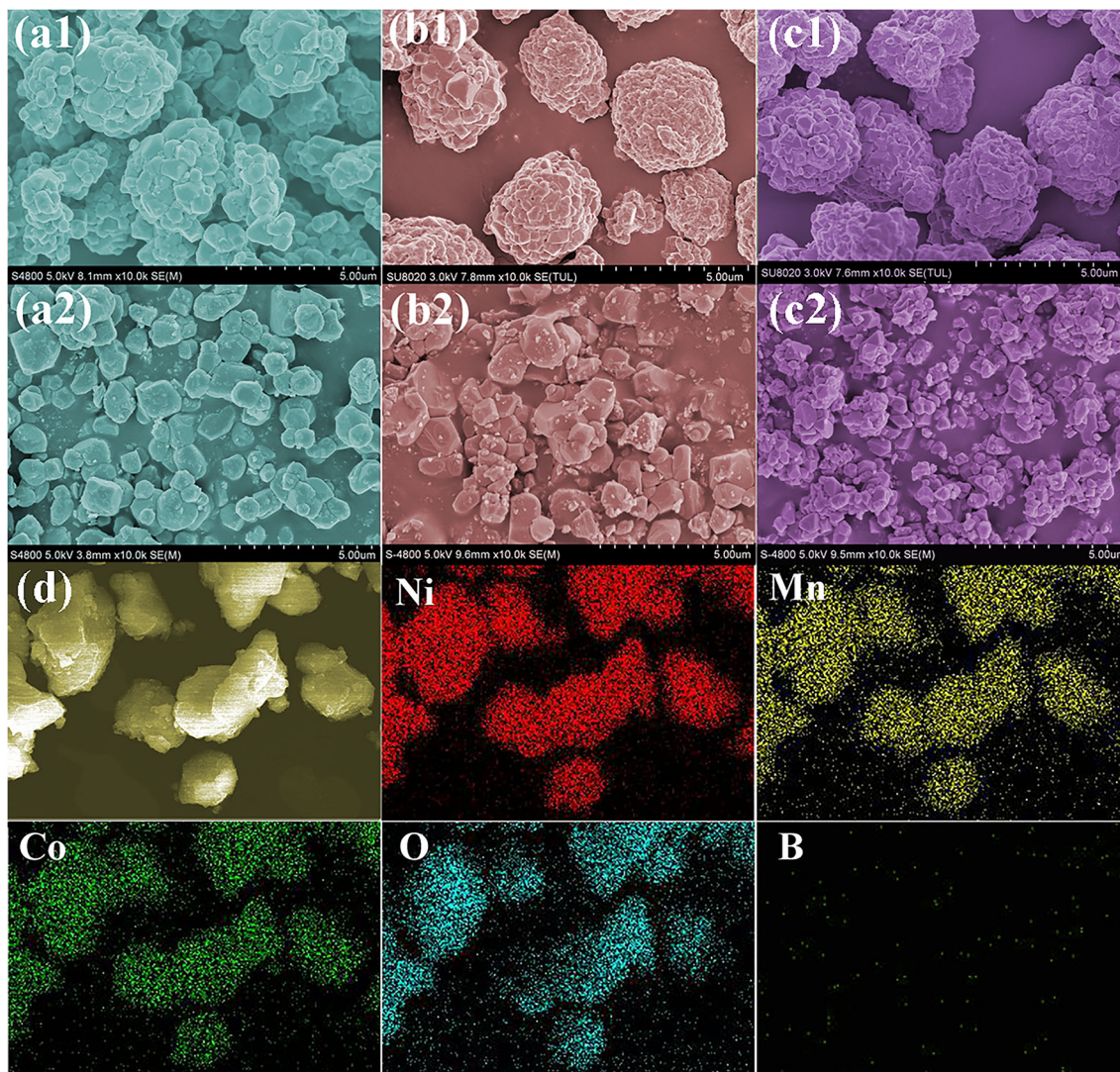


**Fig. 1** FESEM images of a1 A-0.0, a2 S-0.0, b1 A-0.5, b2 S-0.5, c1 A-1.0, c2 S-1.0, and d EDS spectrum of S-0.5

and S-1.0). It is obvious that A-0.0, A-0.5, and A-1.0 are composed of agglomerated secondary particles. After ball milling and reheating process, the agglomerated secondary particles become dispersed single-crystal primary particles as shown in Fig. 1 (a2, b2, and c2). The average particle size of single crystal particles is approximately 0.8–1.5  $\mu\text{m}$ . It is reported that small particle size shorten the lithium-ion migration path, which is conducive to improving rate performance of material [29, 30]. The element distribution on the surface of S-0.5 is examined by EDS mapping, and the results are shown in Fig. 1(d). EDS mapping exhibits Ni, Co, Mn, O, and B elements are homogeneously distributed on the surface of the materials, which proves that boron-doped cathode material with homogeneous element distribution is successfully prepared through our synthetic method.

Figure 2 presents XRD patterns of S-0.0, S-0.5, and S-1.0. The lattice parameters  $a$  and  $c$  are calculated by Jade 6.0 software, and the results are shown in Table 1. Obviously, all

diffraction peaks show that the materials have hexagonal  $\alpha\text{-NaFeO}_2$  structure with  $R3m$  space group and no extra diffraction peaks of impurities exist. The (006)/(102) and (108)/(110) peaks are significantly split, which suggest all the materials possess highly ordered layered structure [31]. All of these indicate that boron doping does not change the hexagonal layer structure. The  $I_{(003)}/I_{(104)}$  reflects the mixing degree of lithium ions and nickel ions in the layered hexagonal structure, and the higher the value of  $I_{(003)}/I_{(104)}$ , the lower the cation mixing degree of the material [32, 33]. S-0.5 exhibits the maximum  $I_{(003)}/I_{(104)}$  value, which indicates it will possess an excellent electrochemical performance. This can be attributed to that boron doping facilitates the formation of layered structures by lowering the crystallization temperature of the layered structure [21]. The (003) diffraction peaks are amplified and inserted in the right of Fig. 2. Apparently, (003) diffraction peaks of S-0.5 and S-1.0 are obviously shifted to a low degree when compared with S-0.0. This implies the unit

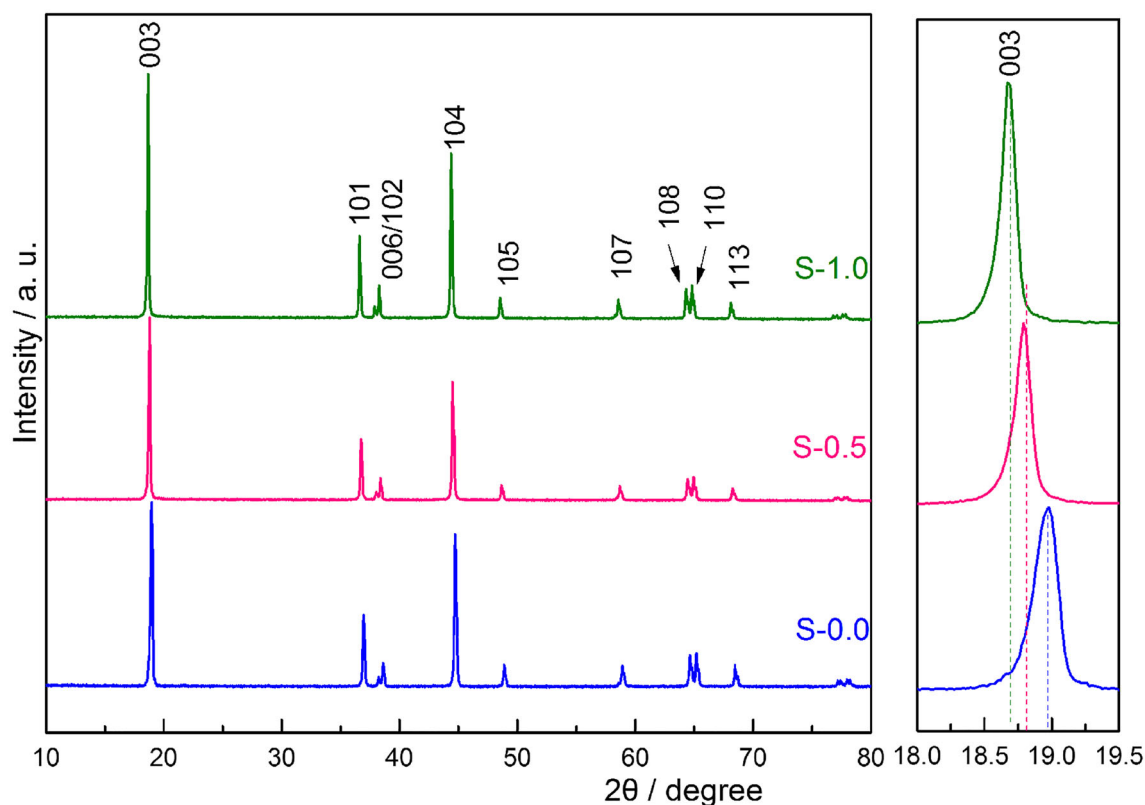


Fig. 2 XRD patterns of S-0.0, S-0.5, and S-1.0

cell is expanded along the  $c$ -direction, and the corresponding lattice parameter  $c$  is also enlarged after boron doping [34]. Similar phenomenon (enlarged parameters) can be found in boron-doped  $\text{LiV}_3\text{O}_8$  and  $\text{Li}_{1.2}\text{Ni}_{0.13}\text{Co}_{0.13}\text{Mn}_{0.54}\text{O}_2$  [14, 16]. Such increased  $c$  indicates expanded pathways for the lithiation/delithiation in the substituted samples, which will be beneficial to the transportation of lithium ions and greatly improve rate performance [35–37]. This will be proved in subsequent electrochemical tests. Generally, the value of  $c/a$  is an indicator for the order of the layered structure. The high  $c/a$  value means that all materials have a well-ordered layered structure. S-0.5 processes the highest  $c/a$  value, which indicates it has the largest channels for lithium-ion intercalation and deintercalation transportation process [38]. The changes of lattice parameters prove that boron is successfully incorporated into the material bulk and beneficial to the electrochemical performance.

**Table 1** Lattice parameters of S-0.0, S-0.5 and S-1.0

Samples	$a(\text{\AA})$	$c(\text{\AA})$	$c/a$	$I_{(003)}/I_{(104)}$
S-0.0	2.8604	14.0362	4.9071	1.2487
S-0.5	2.8455	14.1051	4.9570	1.5154
S-1.0	2.8751	14.2356	4.9513	1.4512

## Electrochemical discussion

The first charge/discharge curves of S-0.0, S-0.5, and S-1.0 charged and discharged at 0.1 C ( $1.0 \text{ C} = 200 \text{ mA g}^{-1}$ ) are presented in Fig. 3a. All samples show similar charge and discharge curves, which indicate that the boron doping in the cathode materials has no significant effect on the charge/discharge properties of  $\text{LiNi}_{0.6}\text{Mn}_{0.2}\text{Co}_{0.2}\text{O}_2$ . The first discharge capacity of S-0.0 is  $197.1 \text{ mAh g}^{-1}$ , while that of S-0.5 and S-1.0 is  $190.7$  and  $182.5 \text{ mAh g}^{-1}$ , respectively. The reduced discharge capacity of the doped samples is attributed to that the doped boron element does not have electrochemical activity, so the doped boron in the cathode material reduces the content of electrochemical active material in the final electrode. Such similar phenomenon can be found in boron-doped cathode materials [15]. The discharge capacity of these samples is higher than the most reports of  $\text{LiNi}_{0.6}\text{Mn}_{0.2}\text{Co}_{0.2}\text{O}_2$ , which may be due to that the single-crystal morphology provides small particle size and smooth particle surface, which can promote the deintercalation efficiency of lithium ions.

Rate capability is one of the important factors of lithium-ion batteries. The charge/discharge curves and capacity retention of S-0.5 and S-1.0 charged at 0.1 C, and then discharged at 0.1 C, 2.0 C, 3.0 C, and 5.0 C, are displayed in Fig. 3b, c, respectively. As shown in Fig. 3b, the discharge capacities of

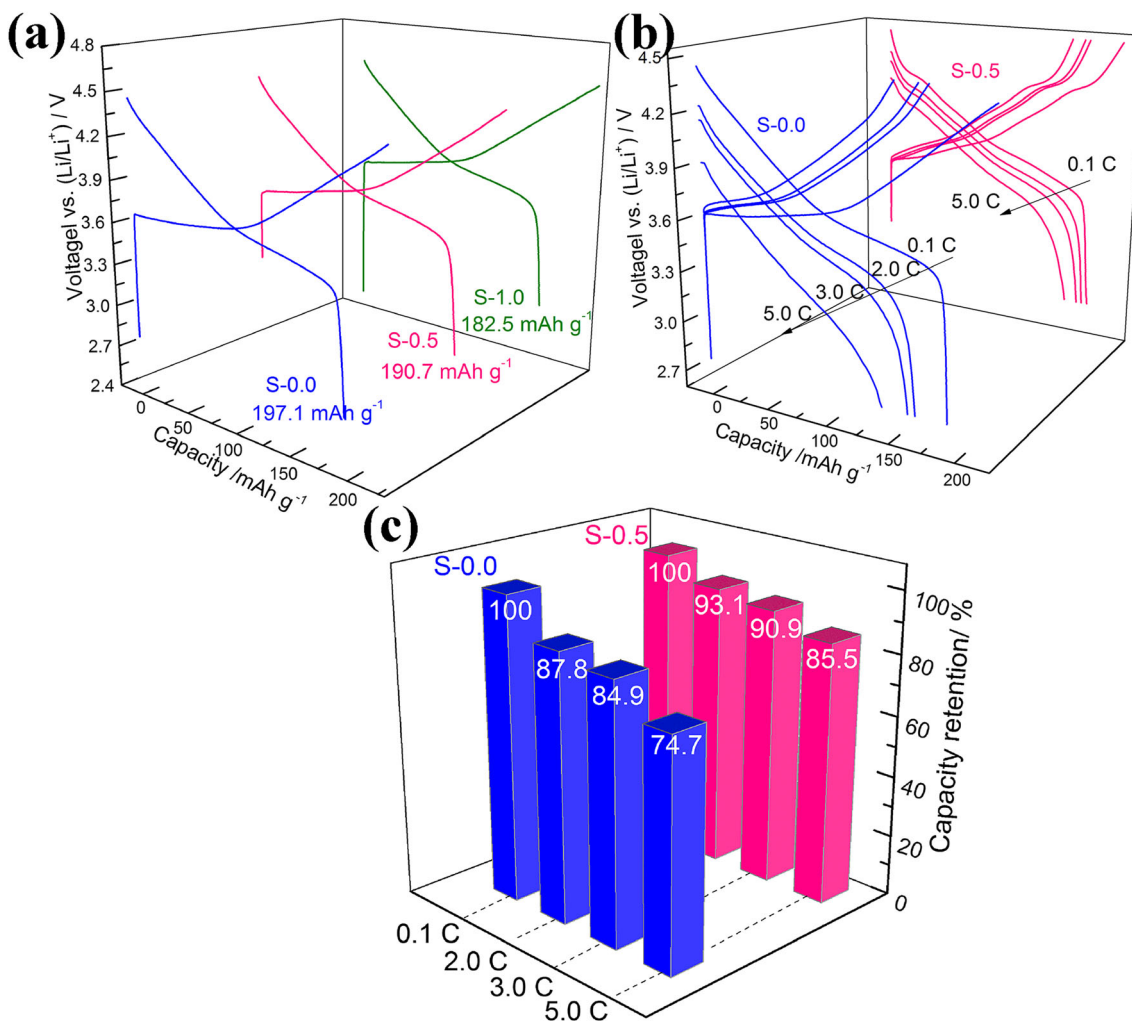


**Fig. 3** a Initial charge/discharge voltage profiles at 0.1 C. b Charge/discharge curves. c Discharge capacity retention rate at 0.1 C, 2.0 C, 3.0 C, and 5.0 C

all the samples decreased gradually with the increases of discharge current rate. In contrast to S-0.0, S-0.5 exhibits distinct improved rate capacity, especially at high current rates. As observed from the charge/discharge profiles at different C-rates (Fig. 3b), S-0.0 shows much stronger electrode polarization with increasing current rate and its potential plateau even disappears at 5.0 C. However, these unfavorable trends are remarkably suppressed in S-0.5. At 0.1 C, S-0.5 shows that a little lower discharge capacity than S-0.0 for boron is electrochemically inactive element. When the discharge rate increases to 2.0 C, the discharge capacity of S-0.0 drops off dramatically to 170.5  $\text{mAh g}^{-1}$ , which is lower than that of S-0.5 (173.0  $\text{mAh g}^{-1}$ ). As the discharge rate continues to increase to 3.0 C, the discharge capacity of S-0.5 reaches 173.0  $\text{mAh g}^{-1}$  with the capacity retention of 90.9% when compared to the discharge capacity at 0.1 C. By contrast, S-0.0 exhibits lower discharge capacity of 164.9  $\text{mAh g}^{-1}$  at 3.0 C, which is 84.9% of the discharge capacity at 0.1 C. With the further increases of discharge current rate to 5.0 C, the excellent performance of S-0.5 is more obvious. S-0.5

possesses a higher discharge capacity of 162.8  $\text{mAh g}^{-1}$  at 5.0 C, which is 85.5% of its discharge capacity at 0.1 C. In comparison, S-0.0 delivers a much lower discharge capacity of 145.2  $\text{mAh g}^{-1}$  at 5.0 C, which is only 74.7% of its discharge capacity at 0.1 C. It is worth noting that the discharge capacity of S-0.5 is higher than that of S-0.0 at high current rate; such similar phenomenon has also been reported in other literatures [12, 39, 40]. From these data comparisons, it is clear that boron doping plays a positive effect on the rate performance. The improved rate performance for S-0.5 is largely attributed to the enlarged (003) plane as mentioned in the XRD analysis section, which decreases the energy barrier for  $\text{Li}^+$  intercalation and deintercalation. Besides that, low cation mixing degree in S-0.5 can provide more electrochemical active ion  $\text{Ni}^{2+}/\text{Ni}^{3+}$  and prevent the structural collapse of the Li layer during the cycling, which also helps improve the rate capability [41, 42]. The results show that boron doping has positive effect on rate performance.

Figure 4 reveals the charge/discharge curves and cycling performance of S-0.0, S-0.5, and S-1.0 at 1.0 C. From the

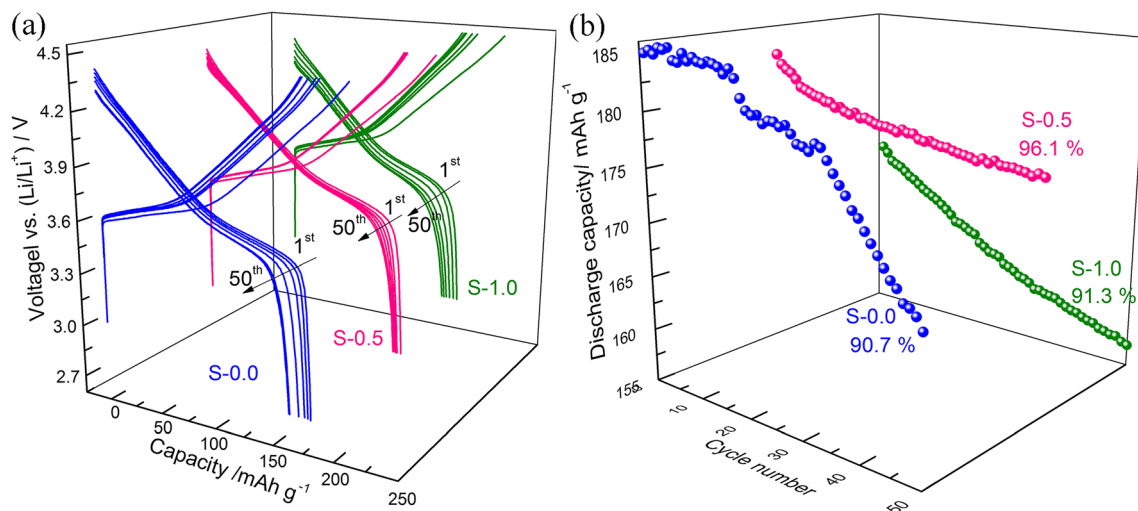


**Fig. 4** **a** Charge/discharge curves at 1.0 C. **b** Cyclic performance of S-0.0, S-0.5, and S-1.0 at 1.0 C

charge/discharge curves (Fig. 4a), it can be observed clearer and steadier charge/discharge plateaus in the profiles of the doped electrodes at the 50th cycle. At the 50th cycle, the highest specific capacity of  $176.3 \text{ mAh g}^{-1}$  is obtained for S-0.5, while that of S-0.0 is only  $167.8 \text{ mAh g}^{-1}$ . Increasing the addition of boron seems to cause inferior electrode performance, in which S-1.0 delivers the lowest discharge capacity of  $157.0 \text{ mAh g}^{-1}$  at the 50th cycle. From Fig. 4c, the cycling stability of S-0.5 is obviously improved as compared to S-0.0. After 50 cycles, the capacity retention of S-0.5 is 96.1%, which is higher than that of S-0.0 and S-1.0 (90.7% and 91.3%), respectively. It is reported that one reason for the attenuation of the discharge capacity due to the  $\text{LiPF}_6$ -based electrolyte usually breaks down and the by-product HF will continuously erode the transition metal ions (Ni, Co, Mn) in the lattice of the NCM cathode material [43]. The excellent cycling performance of S-0.5 can be attributed

to the boron doping stabilizing the crystal structure and enhancing the structural stability of the cathode material. The bond of B–O ( $809 \text{ kJ mol}^{-1}$ ) is stronger than Mn–O ( $402 \text{ kJ mol}^{-1}$ ) and Ni–O ( $382 \text{ kJ mol}^{-1}$ ); thus, boron doping into the crystal structure can play an important role in enhancing the structural stability without blocking the reversibility of  $\text{Li}^+$  ions [20]. However, over-doping of boron may lead to an unstable material structure and undesired impurity, which eventually cause poor electrochemical performance [44]. In addition to the beneficial effects of boron doping, the lower particle size of single-crystal particles results in even shorter mass transport distances and offers many more possibilities to accommodate the strain induced by electrochemical reactions [45]. Both the advantages of boron doping and single-crystal morphology are combined to contribute to the excellent electrochemical performances of the cathode materials.

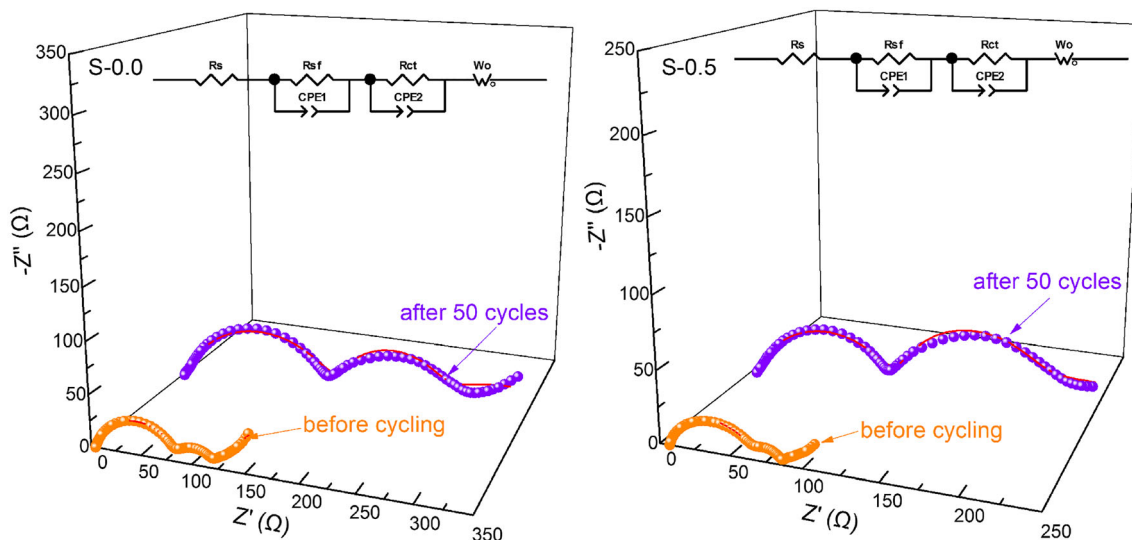


**Fig. 5** EIS plots of S-0.0 and S-0.5 before/after 50 cycles at 4.5 V

**Table 2** Fitting values of the EIS for S-0.0 and S-0.5

Sample	Before the 1st cycle			After the 50th cycle		
	$R_{sf}(\Omega)$	$R_{ct}(\Omega)$	$R_{sf} + R_{ct}(\Omega)$	$R_{sf}(\Omega)$	$R_{ct}(\Omega)$	$R_{sf} + R_{ct}(\Omega)$
S-0.0	81.1	28.6	109.7	175.8	83.9	259.7
S-0.5	56.8	19.5	76.3	94.5	74.0	168.5

Electrochemical impedance spectroscopy (EIS) is an important technique to study the kinetic processes of lithium-ion intercalation/deintercalation in electrodes. EIS of S-0.0 and S-0.5 at charged state of 4.3 V are presented in Fig. 5. The points represent experimental data, and red solid lines are data calculated by Zview2 software. The semicircle in the high frequency represents the SEI film resistance ( $R_{sf}$ ), while the semicircle in the medium frequency stands for the impedance of charge transfer at the interface between the electrolyte and electrode ( $R_{ct}$ ). The slash in the low frequency is related to the diffusion rate of lithium ions in cathode materials ( $W_o$ ) [46]. The equivalent circuits of the EIS spectra are inserted in Fig. 5.  $R_s$  represents solution resistance of the cell, while CEP2 and CEP1 reflect the non-ideal capacitance of surface layer and double layer, respectively. And the resistance values obtained by Zview2 are listed in Table 2. It can be seen that  $R_{sf}$  and  $R_{ct}$  of S-0.5 have been suppressed when compared with that of S-0.0. The suppressed  $R_{sf}$  representing the migration resistance of  $Li^+$  ions through the SEI film is low, and the decreased  $R_{ct}$  indicates small charge transfer resistance through the interface between electrolyte and electrode. During cycling,  $R_{sf}$  of S-0.0 shows faster increase than S-0.5, which grows from 81.1 to 175.8  $\Omega$ . In the contrast,  $R_{sf}$  of S-0.5 is greatly suppressed which only grows from 56.8 to 94.5  $\Omega$ . This represents boron doping can effectively inhibit the sustained decomposition of electrolyte on the surface of the

cathode and then can suppress the growth of SEI film to a large extent. Furthermore, the increase of  $R_{ct}$  is also depressed by boron doping during cycling. For example,  $R_{ct}$  of S-0.5 only increases from 19.5 to 74.0  $\Omega$ . In contrast,  $R_{ct}$  of S-0.0 increases sharply from 28.6 to 83.9  $\Omega$ . Cathode materials directly exposed to electrolyte will cause the dissolution of transition of metal ions and generation of impure phases during cycling process, which result in a sharp increase in the charge transfer resistance [47]. Therefore, the undesirable side reactions between the electrode and electrolyte have been effectively suppressed for the doped sample, and the suppressed SEI film and charge transfer resistances are showed after cycling. Hence, cyclic performance of S-0.5 are greatly improved.

As analyzed in the EIS section, migration of lithium ions within the material phase is reflected in the straight sloping line at low frequency region in the impedance spectrum. As a result, the diffusion coefficient of lithium ions ( $D_{Li^+}$ ) can be obtained by slope of straight line in the low-frequency region by the following formula [48]:

$$D_{Li^+} = \frac{R^2 T^2}{2n^4 F^4 A^2 C_{Li^+}^2 \sigma^2} \tag{1}$$

In the formula,  $n$  is the number of electrons per molecule during electrochemical reaction process,  $F$  represents the Faraday constant,  $A$  refers to the active surface area of the electrochemical reaction (here is surface area of the electrode),  $C_{Li^+}$  is the concentration of lithium ions in materials,  $R$  is the gas constant,  $T$  is the absolute temperature, and  $\sigma$  stands for the Warburg factor which can be calculated by the following formula:

$$Z' = R_s + R_{ct} + \sigma \omega^{-1/2} \tag{2}$$

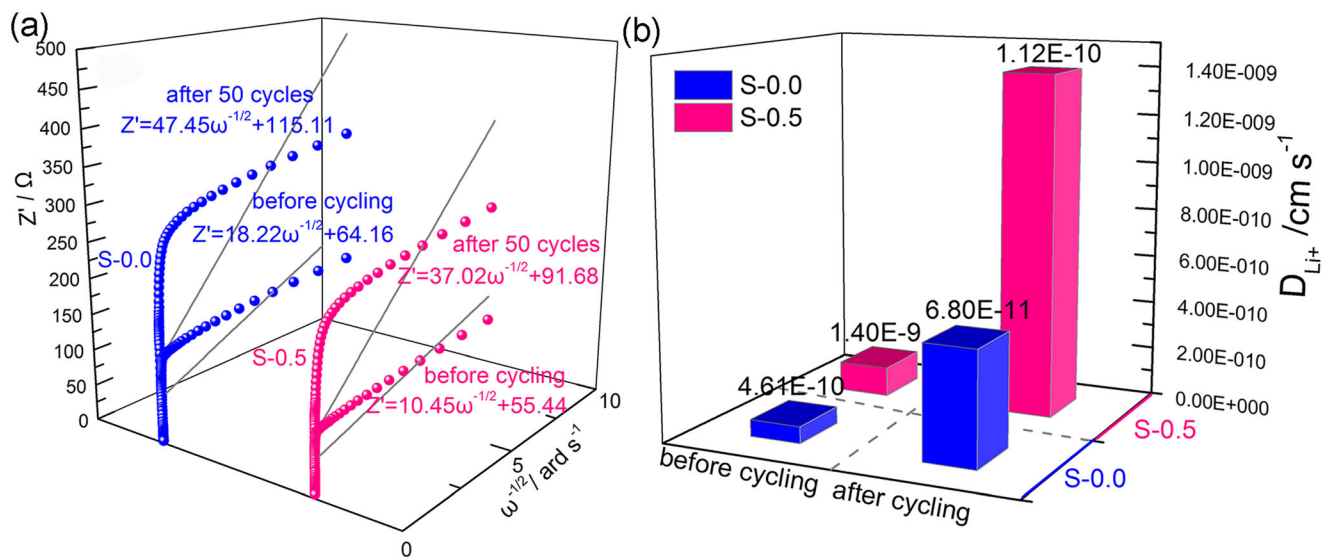


**Fig. 6** a The profiles of  $Z'$  vs.  $\omega^{-1/2}$ . b The corresponding  $D_{Li^+}$  obtained from the EIS data

$Z'$ ,  $R_s$ ,  $R_{ct}$ , and  $\omega$  stand for the real part of impedance, electrolyte resistance, charge transfer resistance, and angular frequency, respectively. The linear relationship of  $Z'$  and  $\omega^{-1/2}$  are shown in Fig. 6a, and the slope of the fitted straight line indicates  $\sigma$  value. According to the formula (1) and (2),  $D_{Li^+}$  can be calculated and compared in Fig. 6b. The obtained  $D_{Li^+}$  of S-0.5 is  $1.40 \times 10^{-9} \text{ cm s}^{-1}$ , which is higher than that of S-0.0 ( $4.61 \times 10^{-10} \text{ cm s}^{-1}$ ). After 50 cycles,  $D_{Li^+}$  value significantly decreases to  $6.8 \times 10^{-11} \text{ cm s}^{-1}$  for S-0.0, while that of S-0.5 only drops to  $1.12 \times 10^{-10} \text{ cm s}^{-1}$ . This indicates that lithium ions migrate more smoothly in S-0.5, which is consistent with the improved rate capability. Since boron doping can suppress the side reactions between cathode material and electrolyte, the structural stability of the cathode material is maintained; thus, the lithium-ion migration rate after 50 cycles is not obviously reduced.

## Conclusion

Boron-doped  $\text{LiNi}_{0.6}\text{Mn}_{0.2}\text{Co}_{0.2}\text{O}_2$  cathode material with single-crystal morphology is prepared via a facile solid-phase sintering method followed by ball milling and reheating process. Compared with pristine sample, the boron-doped sample shows a greatly enhanced rate and cycling performance. Since boron is inserted into lattice of  $\text{LiNi}_{0.6}\text{Mn}_{0.2}\text{Co}_{0.2}\text{O}_2$ , the lattice parameter  $c$  is enlarged which expands pathways for the lithiation/delithiation and beneficial to the transportation of lithium ions. Besides that, strong B–O bond also stabilizes layered structure and enhances cycling performance. Apart from structural stabilization brought by doping effects, we believe that the unique single crystal morphology also contributes to the outstanding performance for its fast lithium-ion transportation as a result of small particle size. Moreover, the incorporated boron also plays a positive role on suppressing the formation of SEI film with low charge transfer resistance. Thus, we believe that this single-crystal boron-doped cathode material with excellent performance is a good candidate for lithium-ion batteries.

**Funding information** This work was supported by the National Natural Science Foundation of China (Grant No. 51772119 and 51202083).

## References

- Manthiram A, Song B, Li W (2017) A perspective on nickel-rich layered oxide cathodes for lithium-ion batteries. *Energy Storage Mater* 6:125–139
- Zhang J, Yang Z, Gao R, Gu L, Hu Z, Liu X (2017) Suppressing the structure deterioration of Ni-rich  $\text{LiNi}_{0.8}\text{Co}_{0.1}\text{Mn}_{0.1}\text{O}_2$  through atom-scale interfacial integration of self-forming hierarchical spinel layer with Ni gradient concentration. *ACS Appl Mater Interfaces* 9:29794–29803
- Hwang S, Jo E, Chung KY, Hwang KS, Kim SM, Chang W (2017) Structural evolution of  $\text{Li}_x\text{Ni}_y\text{Mn}_z\text{Co}_{1-y-z}\text{O}_2$  cathode materials during high-rate charge and discharge. *J Phys Chem Lett* 8:5758–5763
- Zhang H, Karki K, Huang Y, Whittingham MS, Stach EA, Zhou G (2017) Atomic insight into the layered/spinel phase transformation in charged  $\text{LiNi}_{0.80}\text{Co}_{0.15}\text{Al}_{0.05}\text{O}_2$  cathode particles. *J Phys Chem C* 121:1421–1430
- Chen Y, Zhang Y, Chen B, Wang Z, Lu C (2014) An approach to application for  $\text{LiNi}_{0.6}\text{Co}_{0.2}\text{Mn}_{0.2}\text{O}_2$  cathode material at high cutoff voltage by  $\text{TiO}_2$  coating. *J Power Sources* 256:20–27
- Huang B, Li X, Wang Z, Guo H, Shen L, Wang J (2014) A comprehensive study on electrochemical performance of Mn-surface-modified  $\text{LiNi}_{0.8}\text{Co}_{0.15}\text{Al}_{0.05}\text{O}_2$  synthesized by an in situ oxidizing-coating method. *J Power Sources* 252:200–207
- Waller GH, Brooke PD, Rainwater BH, Lai SY, Hu R, Ding Y, Alamgir FM, Sandhage KH, Liu ML (2016) Structure and surface chemistry of  $\text{Al}_2\text{O}_3$  coated  $\text{LiMn}_2\text{O}_4$  nanostructured electrodes with improved lifetime. *J Power Sources* 306:162–170
- Wang M, Gong Y, Gu Y, Chen Y, Chen L, Shi H (2019) Effects of fast lithium-ion conductive coating layer on the nickel rich layered oxide cathode material. *Ceram Int* 45:3177–3185
- Ran Q, Zhao H, Hu Y, Shen Q, Liu W, Liu J, Shu X, Zhang M, Liu S, Tan M, Li H, Liu X (2018) Enhanced electrochemical performance of dual-conductive layers coated Ni-rich  $\text{LiNi}_{0.6}\text{Co}_{0.2}\text{Mn}_{0.2}\text{O}_2$  cathode for Li-ion batteries at high cut-off voltage. *Electrochim Acta* 289:82–93
- Huang B, Lin X, Wang Z, Guo H, Xiong X (2014) Synthesis of Mg-doped  $\text{LiNi}_{0.8}\text{Co}_{0.15}\text{Al}_{0.05}\text{O}_2$  oxide and its electrochemical behavior in high-voltage lithium-ion batteries. *Ceram Int* 40:13223–13230
- Dixit M, Markovsky B, Aurbach D, Major DT (2017) Unraveling the effects of Al doping on the electrochemical properties of  $\text{LiNi}_{0.5}\text{Co}_{0.2}\text{Mn}_{0.3}\text{O}_2$  using first principles. *J Electrochem Soc* 164:A6359–A6365
- Schipper F, Dixit M, Kovacheva D, Talianker M, Haik O, Grinblat J, Erickson EM, Ghanty C, Major DT, Markovsky B, Aurbach D (2016) Stabilizing nickel-rich layered cathode materials by a high-charge cation doping strategy: zirconium-doped  $\text{LiNi}_{0.6}\text{Co}_{0.2}\text{Mn}_{0.2}\text{O}_2$ . *J Mater Chem A* 4:16073–16084
- Hu CL, Yi HH, Wang FX, Xiao SY, Wu YP, Wang D, He DL (2014) Boron doping at P-site to improve electrochemical performance of  $\text{LiMnPO}_4$  as cathode for lithium ion battery. *J Power Sources* 255:355–359
- Feng Y, Li Y, Hou F (2009) Boron doped lithium trivanadate as a cathode material for an enhanced rechargeable lithium ion batteries. *J Power Sources* 187:224–228
- Ebin B, Lindbergh G, Gürmen S (2015) Preparation and electrochemical properties of nanocrystalline  $\text{LiB}_x\text{Mn}_{2-x}\text{O}_4$  cathode particles for Li-ion batteries by ultrasonic spray pyrolysis method. *J Alloys Compd* 620:399–406
- Li B, Yan H, Ma J, Yu P, Xia D, Huang W, Chu W, Wu Z (2014) Manipulating the electronic structure of Li-rich manganese-based oxide using polyanions: towards better electrochemical performance. *Adv Funct Mater* 24:5112–5118
- Alcantara R, Lavela P, Tirado JL (1997) Structure and electrochemical properties of boron-doped  $\text{LiCoO}_2$ . *J Solid State Chem* 134:265–273
- Pan L, Xia Y, Qiu B, Zhao H, Guo H, Jia K, Gu Q, Liu Z (2016) Structure and electrochemistry of B doped  $\text{Li}(\text{Li}_{0.2}\text{Ni}_{0.13}\text{Co}_{0.13}\text{Mn}_{0.54})_{1-x}\text{B}_x\text{O}_2$  as cathode materials for lithium-ion batteries. *J Power Sources* 327:273–280
- Peng Z, Mu K, Cao Y, Xu L, Du K, Hu G (2019) Enhanced electrochemical performance of layered Li-rich cathode materials for lithium ion batteries via aluminum and boron dual-doping. *Ceram Int* 45:4184–4192
- Uzun D (2015) Boron-doped  $\text{Li}_{1.2}\text{Mn}_{0.6}\text{Ni}_{0.2}\text{O}_2$  as a cathode active material for lithium ion battery. *Solid State Ionics* 281:73–81



21. Liu J, Wang S, Ding Z, Zhou R, Xia Q, Zhang J, Chen L, Wei W, Wang P (2016) The effect of boron doping on structure and electrochemical performance of lithium-rich layered oxide materials. *ACS Appl Mater Interfaces* 8:18008–18017
22. Xiao L, Guo Y, Qu D, Deng B, Liu H, Tang D (2013) Influence of particle sizes and morphologies on the electrochemical performances of spinel  $\text{LiMn}_2\text{O}_4$  cathode materials. *J Power Sources* 225:286–292
23. Ryu WH, Lim SJ, Kim WK, Kwon HS (2014) 3-D dumbbell-like  $\text{LiNi}_{1/3}\text{Mn}_{1/3}\text{Co}_{1/3}\text{O}_2$  cathode materials assembled with nano-building blocks for lithium-ion batteries. *J Power Sources* 257:186–191
24. Kim Y (2012) Lithium nickel cobalt manganese oxide synthesized using alkali chloride flux: morphology and performance as a cathode material for lithium ion batteries. *ACS Appl Mater Interfaces* 4:2329–2333
25. Feng J, Wang Y (2016) High-rate and ultralong cycle-life  $\text{LiFePO}_4$  nanocrystals coated by boron-doped carbon as positive electrode for lithium-ion batteries. *Appl Surf Sci* 390:481–488
26. Arico AS, Bruce P, Scrosati B, Tarascon JM, Schalkwijk WV (2005) Nanostructured materials for advanced energy conversion and storage devices. *Nat Mater* 4:1027–1034
27. Lee KT, Cho J (2011) Roles of nanosize in lithium reactive nanomaterials for lithium ion batteries. *Nano Today* 6:28–41
28. Sun C, Rajasekhara S, Goodenough JB, Zhou F (2011) Monodisperse porous  $\text{LiFePO}_4$  microspheres for a high power Li-ion battery cathode. *J Am Chem Soc* 133:2132–2135
29. Hwang I, Lee CW, Kim JC, Yoon S (2012) Particle size effect of Ni-rich cathode materials on lithium ion battery performance. *Mater Res Bull* 47:73–78
30. Nara H, Morita K, Mukoyama D, Yokashima T, Momma T, Osaka T (2017) Impedance analysis of  $\text{LiNi}_{1/3}\text{Mn}_{1/3}\text{Co}_{1/3}\text{O}_2$  cathodes with different secondary-particle size distribution in lithium-ion battery. *Electrochim Acta* 241:323–330
31. Jiang X, Sha Y, Cai R, Shao Z (2015) The solid-state chelation synthesis of  $\text{LiNi}_{1/3}\text{Co}_{1/3}\text{Mn}_{1/3}\text{O}_2$  as a cathode material for lithium-ion batteries. *J Mater Chem A* 3:10536–10544
32. Zhang X, Mauger A, Qi L, Grout H, Perrigaud L (2010) Synthesis and characterization of  $\text{LiNi}_{1/3}\text{Mn}_{1/3}\text{Co}_{1/3}\text{O}_2$  by wet-chemical method. *Electrochim Acta* 55:6440–6449
33. Li N, An R, Su Y, Wu F, Bao L, Chen L, Zheng Y, Shou H, Chen S (2013) The role of yttrium content in improving electrochemical performance of layered lithium-rich cathode materials for Li-ion batteries. *J Mater Chem A* 1:9760–9767
34. Song G, Zhong H, Dai Y, Zhou X, Yang J (2019)  $\text{WO}_3$  membrane-encapsulated layered  $\text{LiNi}_{0.6}\text{Co}_{0.2}\text{Mn}_{0.2}\text{O}_2$  cathode material for advanced Li-ion batteries. *Ceram Int* 45:6774–6781
35. Yoon WS, Chung KY, Mcbreen J, Yang XQ (2006) A comparative study on structural changes of  $\text{LiCo}_{1/3}\text{Ni}_{1/3}\text{Mn}_{1/3}\text{O}_2$  and  $\text{LiNi}_{0.8}\text{Co}_{0.15}\text{Al}_{0.05}\text{O}_2$  during first charge using in situ XRD. *Electrochem Commun* 8:1257–1262
36. Ryu HH, Park KJ, Yoon CS, Sun YK (2018) Capacity fading of Ni-rich  $\text{Li}[\text{Ni}_x\text{Co}_y\text{Mn}_{1-x-y}]\text{O}_2$  ( $0.6 \leq x \leq 0.95$ ) cathodes for high energy density lithium-ion batteries: bulk or surface degradation? *Chem Mater* 30:1155–1163
37. Li L, Zhang Z, Fu S, Liu Z (2019) F127-assisted synthesis of  $\text{LiNi}_{0.5}\text{Co}_{0.2}\text{Mn}_{0.3}\text{O}_{1.99}\text{F}_{0.01}$  as a high rate and long life span cathode material for lithium-ion batteries. *Appl Surf Sci* 476:1061–1071
38. Yuan H, Song W, Wang M, Gu Y, Chen Y (2019) Lithium-ion conductive coating layer on nickel rich layered oxide cathode material with improved electrochemical properties for Li-ion battery. *J Alloys Compd* 784:1311–1322
39. Liu Q, Su X, Lei D, Qin Y, Wen J, Guo F, Wu YA, Rong Y, Kou R, Xiao X, Aguesse F, Barenjo J, Ren Y, Lu W, Li Y (2018) Approaching the capacity limit of lithium cobalt oxide in lithium ion batteries via lanthanum and aluminium doping. *Nat Energy* 3:936–943
40. Zhao J, Wang Z, Wang J, Guo H, Li X, Gui W, Chen N, Yan G (2018) Anchoring  $\text{K}^+$  in  $\text{Li}^+$  sites of  $\text{LiNi}_{0.8}\text{Co}_{0.15}\text{Al}_{0.05}\text{O}_2$  cathode material to suppress its structural degradation during high-voltage cycling. *Energ Technol* 3:936–943
41. Huang Z, Wang Z, Jing Q, Guo H, Li X, Yang Z (2016) Investigation on the effect of Na doping on structure and Li-ion kinetics of layered  $\text{LiNi}_{0.6}\text{Co}_{0.2}\text{Mn}_{0.2}\text{O}_2$  cathode material. *Electrochim Acta* 192:120–126
42. Kiziltas-Yayuz N, Yavuz M, Indris S, Bramnik NN, Knapp M, Dolotko O, Das B, Ehrenberg H, Bhaskar A (2016) Enhancement of electrochemical performance by simultaneous substitution of Ni and Mn with Fe in Ni-Mn spinel cathodes for Li-ion batteries. *J Power Sources* 327:507–518
43. Ran Q, Zhao H, Wang Q, Shu X, Hu Y, Hao S, Wang M, Liu J, Zhang M, Li H, Liu N, Liu X (2019) Dual functions of gradient phosphate polyanion doping on improving the electrochemical performance of Ni-rich  $\text{LiNi}_{0.6}\text{Co}_{0.2}\text{Mn}_{0.2}\text{O}_2$  cathode at high cut-off voltage and high temperature. *Electrochim Acta* 299:971–978
44. Xu H, Deng S, Chen G (2014) Improved electrochemical performance of  $\text{Li}_{1.2}\text{Mn}_{0.54}\text{Ni}_{0.13}\text{Co}_{0.13}\text{O}_2$  by Mg doping for lithium ion battery cathode material. *J Mater Chem A* 36:15015–15026
45. Armstrong AR, Paterson AJ, Robertson AD, Bruce PG (2002) Nonstoichiometric layered  $\text{Li}_x\text{Mn}_y\text{O}_2$  with a high capacity for lithium intercalation/deintercalation. *Chem Mater* 14:710–719
46. He W, Yuan DD, Qian JF, Ai XP, Yang HX, Cao YL (2013) Enhanced high-rate capability and cycling stability of Na-stabilized layered  $\text{Li}_{1.2}[\text{Co}_{0.13}\text{Ni}_{0.13}\text{Mn}_{0.54}]\text{O}_2$  cathode material. *J Mater Chem A* 1:11397–11403
47. Wang X, Yagi Y, Lee YS, Yoshio M, Xia Y, Sakai T (2001) Storage and cycling performance of stoichiometric spinel at elevated temperatures. *J Power Sources* 97-98:427–429
48. Qiao YQ, Tu JP, Wang XL, Zhang J, Yu YX, Gu CD (2011) Self-assembled synthesis of hierarchical waferlike porous Li-V-O composites as cathode materials for lithium ion batteries. *J Phys Chem C* 115:25508–25518

**Publisher's note** Springer Nature remains neutral with regard to jurisdictional claims in published maps and institutional affiliations.